CHINESE OPTICS LETTERS

Vol. 19, No. 7 | July 2021

Ultra-long-period grating-based multi-wavelength ultrafast fiber laser [Invited]

Bo Guo (郭 波)*, Xinyu Guo (郭心宇), Lige Tang (唐李格), Wenlei Yang (杨文蕾)**, Qiumei Chen (尘秋美), and Zhongyao Ren (任忠要)

Key Laboratory of In-fiber Integrated Optics, Ministry of Education, Harbin Engineering University, Harbin 150001, China

*Corresponding author: guobo512@163.com

**Corresponding author: ywl-_-@hotmail.com

Received November 17, 2020 | Accepted January 5, 2021 | Posted Online April 12, 2021

We propose and demonstrate the cascaded multi-wavelength mode-locked erbium-doped fiber laser (EDFL) based on ultra-long-period gratings (ULPGs) for the first time, to the best of our knowledge. Study found that the ULPG can be used as both a mode-locker for pulse shaping and a comb filter for multi-wavelength generation simultaneously. Using the dual-function of ULPG, three-, four-, five-, six-, and seven-wavelength mode-locked pulses are obtained in EDFL, seven of which are the largest number of wavelengths up to now. For the four-wavelength soliton pulses, their pulse width is about 7.8 ps. The maximum average output power and slope efficiency of these pulses are 8.4 mW and 2.03%, respectively. Besides the conventional pulses, hybrid soliton pulses composed of a four-wavelength pulse and single soliton are also observed. Finally, the effect of cavity dispersion on the multi-wavelength mode-locked pulses is also discussed. Our findings indicate that apart from common sensing and filtering, the ULPG may also possess attractive nonlinear pulse-shaping property for ultrafast photonics application.

Keywords: ultra-long-period grating; fiber laser; ultrafast laser; multi-wavelength.

DOI: 10.3788/COL202119.071405

1. Introduction

In the future of ultra-high speed and large-capacity all-optical communication, the laser source used is required to be simple, compact, and have high beam quality, especially with dual functions of mode-locking and multi-wavelength operation. Based on this, multi-wavelength ultrafast photonics has been a very active and important research direction in recent years[1–3]. To obtain the multi-wavelength picosecond/femtosecond pulses, it generally needs to employ an optical comb filter and a mode-locker in the laser cavity simultaneously. For the former, nonlinear optical effects (e.g., four-wave mixing[4], stimulated Brillouin scattering[5]) and real optical devices (e.g., sampling grating[6], Sagnac interferometer[7], Mach–Zehnder interferometer[8]) have been used as comb filters to realize multi-wavelength operation. For the latter, active (acoustic-optic[9] or electro-optic[10] modulation) and passive schemes[11–15] have been developed rapidly. Compared with active mode-locking, passive mode-locking has more advantages, such as simplicity, compactness, and flexible design. With these two devices, multi-wavelength mode-locked lasers can be realized. However, up to now, it is still difficult to obtain multi-wavelength mode-locked pulses with high average output power and large wavelength numbers (> 4) due to the high insertion loss caused by the presence of a mode-locker and a comb filter in the laser cavity. Thus, it is urgent to seek a dual-function device with wavelength-filtering and mode-locking to achieve the high-quality multi-wavelength mode-locked lasers.

In recent years, three kinds of fiber gratings have been developed: fiber Bragg grating, long-period fiber grating, and ultra-long-period grating (ULPG). Among them, the axial effective index in the fiber is periodically modulated by the pitch of millimeter (mm) order, which is called ULPG. From the point of view of the spectrum, there are a series of discrete attenuation bands and a wide periodic distribution in the transmission spectrum[16]. Theoretically, ULPG can couple the propagating light between the fundamental mode and the cladding mode at a certain resonant wavelength under the condition of phase matching. Since the first, to the best of our knowledge, successful fabrication in 2001, the study of ULPGs has been a research hot-spot in the field of optical fibers[17,18]. So far, many fabrication methods of ULPG have been developed[19–23], including amplitude mask, mechanical micro-bend, corrosion groove, and local heating (e.g., electric arc discharge, CO_2 laser irradiation, femtosecond laser exposure, and hydrofluoric etching). As far as application is concerned, the period of ULPG is very long

(mm scale), and the requirement of grating period accuracy is relatively low. Therefore, the fiber devices constructed by using it have the advantages of compact structure, reliable performance, and low price. For example, due to its excellent environmental sensitivity and spectral response[24–29], ULPGs have been used as a variety of optical devices, including sensors[30–35], temporal differentiators[36], Mach–Zehnder interferometers[37], mode converters[38], and filters[39–41].

The application of long-period gratings in fiber lasers is just beginning[42–46]. For example, Han *et al.* and Yan *et al.* obtained the multi-wavelength Raman fiber laser[44] and switchable triple-wavelength fiber laser[45], respectively, by means of a comb filter, which is composed by cascaded long-period gratings. In addition, Liu *et al.* also achieved the tunable and switchable multi-wavelength fiber laser incorporating a polarization-dependent comb filter composed of two cascaded mismatching long-period gratings[46]. They pointed out that the comb filter can be used as both a wavelength selector and a switchable filter. However, it should be noted that the multiple lasing that is mentioned above is continuous wave (CW) and may not be suitable for high-speed optical communication. Interestingly, Intrachat and Kutz proposed theoretically the intensity-dependent mode-coupling dynamics of a long-period grating and pointed out that it could be used to realize mode-locking of fiber lasers[47]. Study found that the long-period grating is sufficient for producing stable mode-locked pulses after many round trips in the laser cavity. Furthermore, Karar *et al.* theoretically investigated the nonlinear pulse dynamics in a passively mode-locked linear cavity erbium-doped fiber laser (EDFL) containing a long-period grating[48]. They predicted the existence of a single soliton, bound soliton, long-period pulsation, coexisting attractor, and multi-soliton pulse in the fiber laser. However, no mode-locked fiber lasers based on long-period gratings have been experimentally studied yet. As mentioned above, the ULPG has more advantages than long-period fiber gratings. Thus, a question arises naturally: can the ULPG operate as both an excellent mode-locker and a comb filter simultaneously? Clearly, the exploration of this problem will help us to expand the application scope of ULPGs.

Here, we achieved the cascaded multi-wavelength mode-locked EDFL, in which the ULPG can operate as both a mode-locker for pulse shaping and a comb filter for the multi-wavelength lasing simultaneously. These findings indicate that the ULPG could become a good candidate of pulse-shaping devices for ultrafast photonics.

2. Fabrication and Characteristics of the ULPG and Its Saturable Absorption

The as-used ULPG was fabricated by using the fused biconical taper technique, which was similar to our previous report[49]. The experimental setup for fabricating the ULPG is illustrated in Fig. 1. The system is mainly composed of the GPX-3000 optical fiber processing system, supercontinuum light source (1450–1650 nm, NKT Photonics), and optical spectrum analyzer

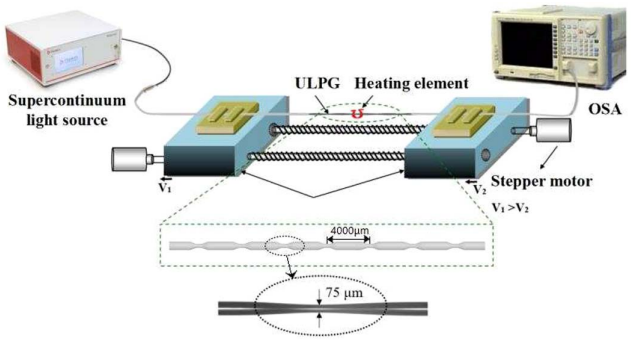

Fig. 1. Schematic diagram of the experimental setup for fabricating the ULPG sample. The green frame is the diagram of the ULPG sample and a micrograph of a fiber taper.

(Yokogawa AQ6370C). The central section was a GPX-3000 glass processing system, in which the power supply and moving speed are about 50 W and 0.3 mm/s, respectively. Initially, the single-mode fiber (SMF) with coating removed is placed horizontally on two clamps, and strain force is applied on both sides of the fiber to make it in a straight state. After the geometric size of the fiber taper is set, the taper is drawn. Under the pulling force, a taper is made locally in the optical fiber. Then, the next taper is made at the new position of the optical fiber by moving the horizontal displacement table. The parameters of the next taper are the same as those of the first taper. The distance between two adjacent tapers is defined as the period length. In the process of fabrication, the two horizontal displacement tables move synchronously under the driving of the stepping motor, which is equivalent to the movement of the heating element (~1 mm wide graphite filament). Meanwhile, the moving speed of the left horizontal displacement table (V_1) is greater than that of the right horizontal displacement table (V_2), which makes the optical fiber maintain the tensile state. In this experiment, a ULPG with seven tapers was obtained, as shown in Fig. 1. It can be seen that the waist diameter, taper length, and the period between two tapers were ~ 75 μm, 2 mm, and 4 mm, respectively.

Next, we provided the transmission spectrum of the as-used ULPG by using the light injection method, as shown in Fig. 2(a). It can be seen that there are two dips centered at 1557.8 nm (λ_1) and 1593.4 nm (λ_2) in the transmission spectrum, respectively, which are consistent with the prediction of coupled mode theory. Theoretically, the two adjacent fiber tapers of the ULPG can be regarded as a Mach–Zehnder interferometer, and the core mode and cladding mode are equivalent to its two arms[45,46]. When the transmitted light interferes with each other, the phase delay will occur after a certain distance, and two adjacent dips will appear in the transmission spectrum. This means that the ULPG can operate well around 1550 nm, and it is very suitable for building C-band and L-band EDFLs. Notably, for a tapered ULPG, the effective refractive index of its waist and core part is different, which can be verified by whether the evanescent field appears when the visible light passes out. In experiment, we can observe it with a yellow light

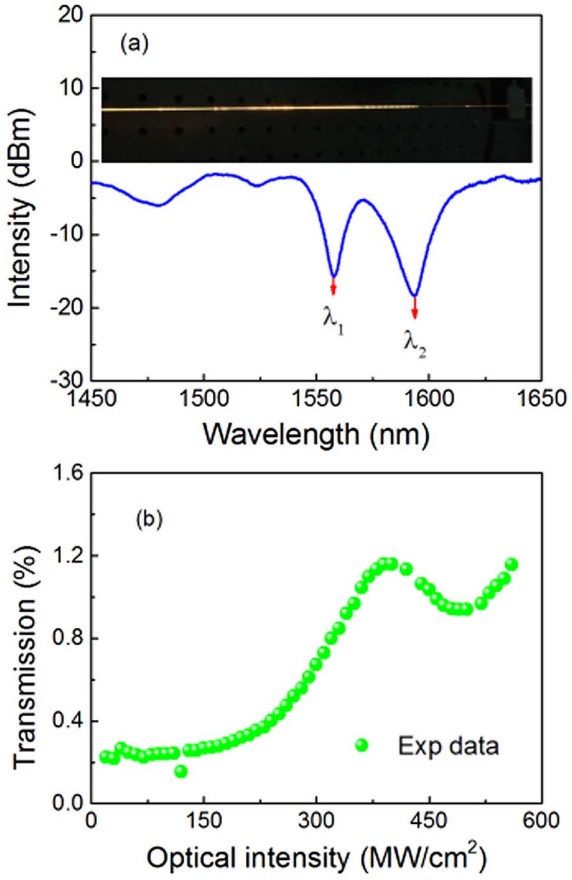

Fig. 2. Typical optical characteristics and saturable absorption property of the as-used ULPG: (a) transmission spectrum (inset: the photograph when the yellow light is passing out); (b) nonlinear saturable absorption behavior.

source, as shown in the inset of Fig. 2(a). Clearly, the profile of the yellow laser beam was not well-distributed due to the existence of the evanescent field.

In this experiment, the saturable absorption behavior of the ULPG played a key role. To this end, we then investigated it with a balanced twin-detector method. The experiment setup was similar to our previous report[50]. The as-used source was a femtosecond fiber laser mode-locked by a semiconductor saturable absorber mirror (SESAM). Its central wavelength, fundamental repetition rate, minimum pulse width, and maximum average output power were 1550 nm, 50 MHz, 50 fs, and 500 mW, respectively. By increasing the pump power gradually, we observed the saturable absorption behavior of the ULPG, which is similar to the previous theoretical result[51]. As seen from Fig. 2(b), the modulation depth and saturation intensity were about 1% and 300 MW/cm^2, respectively. Notably, the transmission of the ULPG was relatively low, which may be caused by the large insertion loss of seven tapers in the ULPG. In this experiment, the insertion loss of the ULPG is about 7.5 dB. In future work, we will further improve the fabrication quality of the fiber taper to obtain a ULPG with a smaller insertion loss.

3. Experimental Setup

To verify the optical property of the prepared ULPG, we transferred it into a ring cavity EDFL. The experimental scheme is illustrated in Fig. 3. The gain medium consisted of a ∼ 4.5 m erbium-doped fiber (Core active L-900, EDF) with a dispersion parameter of ∼ − 16.3 ps/(km·nm). The pump source was a laser diode (LD, 980-420-B-FA) centered at 976 nm, and its maximum output power was 420 mW. The unidirectional operation of the laser beam was achieved by utilizing a polarization-independent isolator in the ring cavity. Meanwhile, we could adjust flexibly the polarization states of the laser beam by using a polarization controller (PC). A variable-length of SMF with a dispersion parameter of ∼18 ps/(km·nm) varies between 20 m and 135 m and was used to adjust the cavity dispersion. Moreover, a 980/1550 wavelength-division multiplexer and a 10:90 optical coupler were used to extract the input and output of the laser beam, respectively. The performance parameters of the laser pulse are measured by a power meter, a spectrum analyzer (ANDO AQ-6317B) with a spectral resolution of 0.01 nm, a photodetector (Thorlabs PDA 12.5 GHz) combined with a 1 GHz mixed oscilloscope (Tektronix MDO4054-6, 5 GHz/s), and a commercial autocorrelator (APE, PulseCheck).

4. Results and Discussion

4.1. Multi-wavelength mode-locked pulses generation

Before carrying out the experiment, we tested the operation characteristic of the fiber laser without incorporating the ULPG in the laser cavity. By adjusting the pump strength and the cavity polarization state in a wide range, there is neither mode-locking nor multi-wavelength generation, which excludes the possibility of self-mode-locking and Fabry–Perot cavity effect. Then, the ULPG was inserted into the cavity (Fig. 3); we observed that the CW and soliton state appeared when the output power from the LD was about 30 and 50 mW, respectively. Next, by flexibly rotating the paddles of the PC, we obtained the three-wavelength soliton pulses when the pump power increased to ∼ 60 mW, a length of SMF of 93.5 m, and

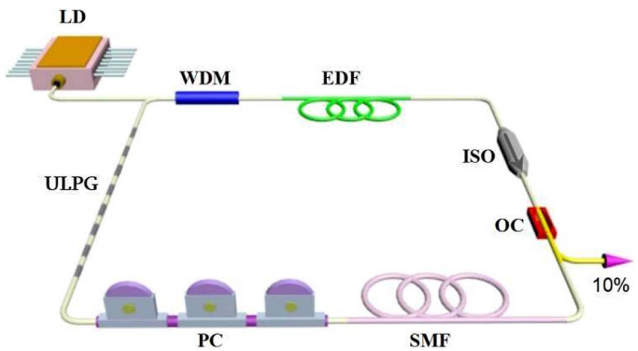

Fig. 3. Experimental setup. LD, laser diode; WDM, wavelength-division multiplexer; EDF, erbium-doped fiber; ISO, isolator; OC, optical coupler; SMF, single-mode fiber; PC, polarization controller; ULPG, ultra-long-period grating.

a corresponding cavity dispersion of $\sim -2.01\,\mathrm{ps}^2$. Its optical spectrum and corresponding pulse train are shown in Fig. 4. As seen in Fig. 4(a), there were three wavelengths that appeared in the range of 3 dB on the whole optical spectrum. Clearly, there are two pairs of Kelly sidebands in the spectrum, which are the feature of the soliton pulse emitted from the laser systems. However, these Kelly sidebands are asymmetrical, which may be caused by the wavelength-filtering and dispersion effect in the laser cavity[52]. In this spectrum, the wavelength interval between two pulses and the 3 dB spectral width were about 0.8 and 0.12 nm, respectively. It should be noted that its central wavelength (1535.3 nm) deviated from the transmission wavelength (1557.8 nm) of the ULPG, which may be related to the large insertion loss of the ULPG as mentioned above. We believe that in the future work this central wavelength can be shifted to around 1550 nm by optimizing the design of the ULPG. In addition, we also provide the pulse train and zoom-in image of a single-pulse profile, as illustrated in Fig. 4(b). Obviously, there were three pulses (marked 1, 2, 3) transmitted in the laser cavity that exhibited the same period of 477 ns, which indicated the fundamental repetition rate of ~ 2.1 MHz. The pulse intervals between two pulses (1 and 2, 2 and 3) were 174 ns and 129 ns, respectively.

Furthermore, we also obtained the four-wavelength soliton mode-locking operation by flexibly adjusting the polarization states through the PC when the pump power was set to 180 mW. It can be seen from Fig. 5(a) that there were three pairs of Kelly sidebands that appeared on both sides of the optical spectrum, which implied that they were soliton pulses. In experiment, we also provided the autocorrelation trace of the single-soliton pulse using a narrow-band filter. Its pulsewidth is about 7.8 ps. In addition, we provided the pulse train and zoom-in image of a single-pulse profile, as shown in Fig. 5(b). It can be seen that four pulses (marked 1, 2, 3, 4) with a 477 ns period are transmitted in the laser cavity, and the pulse intervals between the two pulses (1 and 2, 2 and 3, 3 and 4, 4 and 1) are about 190 ns, 95 ns, 75 ns, and 117 ns, respectively.

In the experiment, we also found that, the multi-wavelength mode-locked pulses were polarization-dependent. For example, the four-, five-, and six-wavelength mode-locking operation could be achieved by properly adjusting the polarization states through the PC under the pump power of 210 mW, as shown in Fig. 6. It can be seen from Figs. 6(a)–6(c) that the wavelength intervals between two pulses and the spectral width within 3 dB were about 0.86 nm, 1.15 nm, 0.98 nm, and 0.24 nm, 0.12 nm, 0.12 nm for the four-, five-, and six-wavelength mode-locked pulses, respectively. Moreover, no sidebands

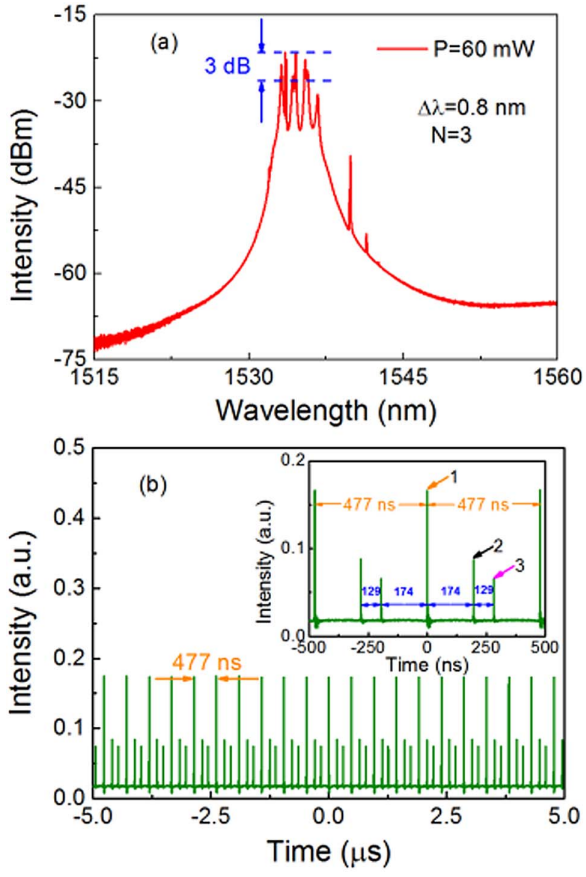

Fig. 4. Three-wavelength soliton mode-locking operation with a length of SMF of 93.5 m and a corresponding cavity dispersion of $\sim -2.01\,\mathrm{ps}^2$. (a) Optical spectrum and (b) the corresponding pulse train (inset: the zoom-in image).

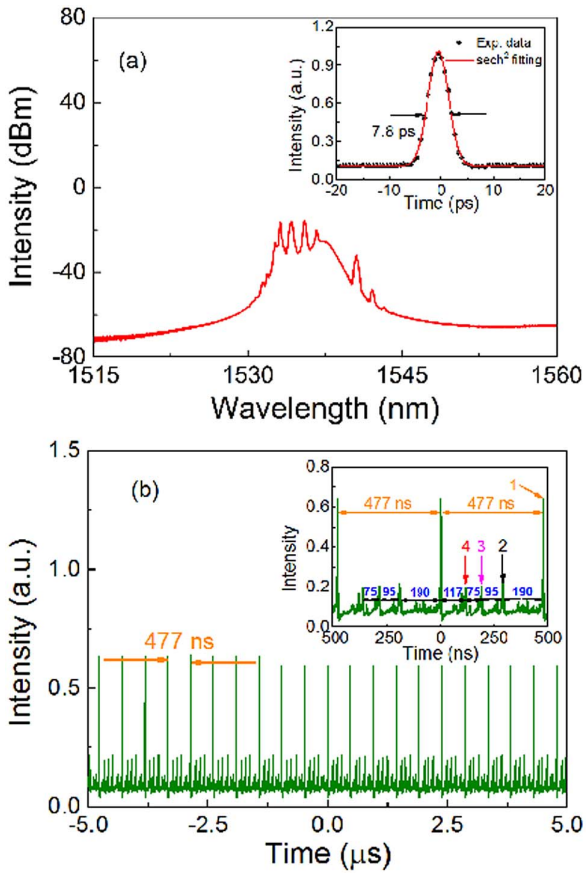

Fig. 5. Four-wavelength soliton mode-locking operation with a length of SMF of 93.5 m and a corresponding cavity dispersion of $\sim -2.01\,\mathrm{ps}^2$. (a) Optical spectrum and (b) the corresponding pulse train (inset: the zoom-in image).

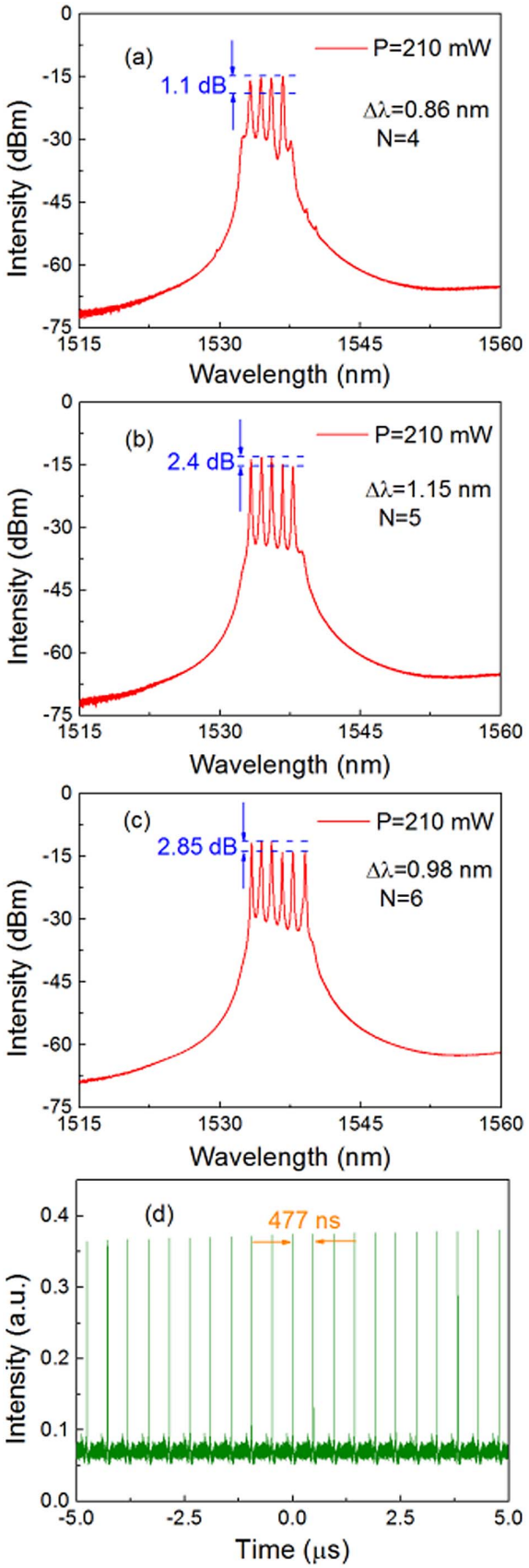

Fig. 6. Multi-wavelength mode-locking operation with a length of SMF of 93.5 m and a corresponding cavity dispersion of $\sim -2.01\,ps^2$. (a) Four-, (b) five-, (c) six-wavelength, and (b) the corresponding pulse train.

appear in the spectrogram, no solitons are formed, and only one pulse is transmitted in the laser cavity. Moreover, Fig. 6(d) shows the corresponding pulse train with a period of about 477 ns.

4.2. Effect of cavity dispersion on multi-wavelength mode-locked pulses

Notably, for the triple-wavelength mode-locking operation, as shown in Fig. 4, their Kelly sidebands were different from those

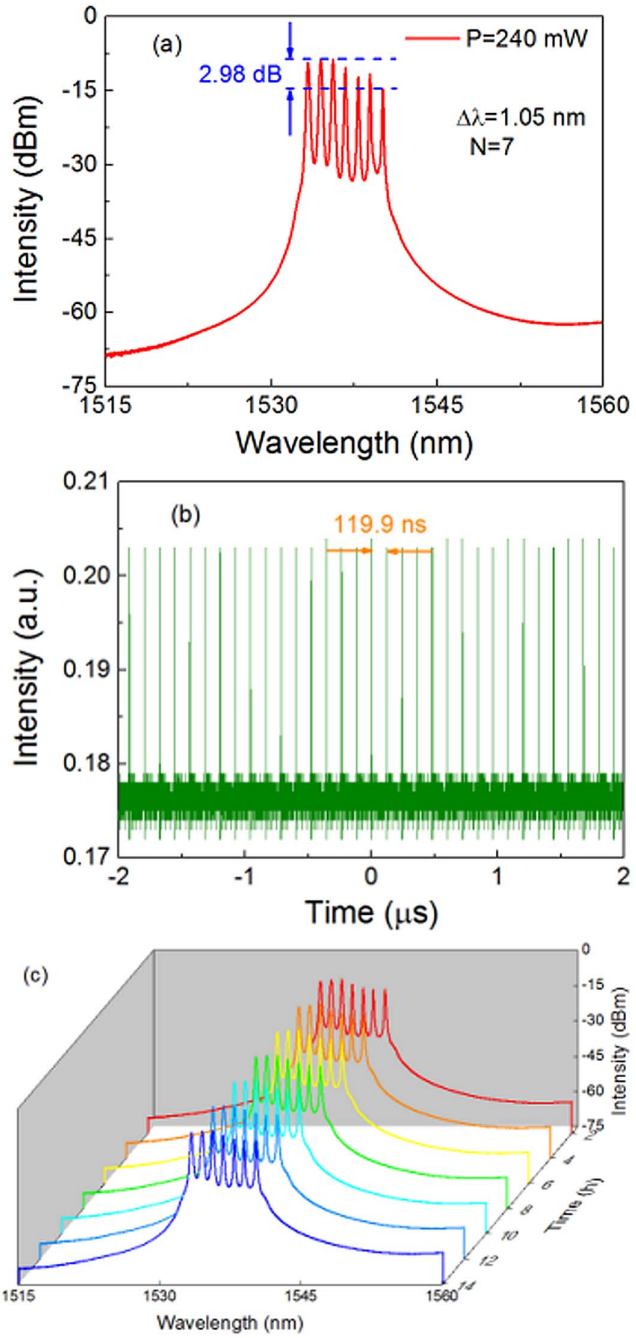

Fig. 7. Seven-wavelength mode-locking operation with a length of SMF of 20 m and a corresponding cavity dispersion of $\sim -0.35\,ps^2$. (a) Optical spectrum, (b) the corresponding pulse train, and (c) long-term optical spectra measured at 2 h intervals over 14 h.

of the soliton pulses, implying that their formation could be affected by the dispersion. Thus, we then discussed the effect of cavity dispersion on the multi-wavelength mode-locked pulses. Here, we studied the dynamics of the multi-wavelength mode-locking operation by properly setting the polarization states through the PC when we decreased the length of the SMF (L_{SMF}) from 93.5 to 20 m. Figure 7 shows the optical spectrum and pulse train of the seven-wavelength mode-locking operation by flexibly adjusting the polarization states through the PC when L_{SMF} was about 20 m, and the corresponding cavity dispersion is $\sim -0.35\ ps^2$. It can be seen from Fig. 7(a) that the wavelength interval between two pulses and the bandwidth within 2.98 dB were about 1.05 and 0.24 nm, respectively. As seen in Fig. 7(b), the pulse train exhibited a period of ~ 119.9 ns, which indicated that the fundamental repetition rate was about 8.34 MHz. In addition, we also provided the evolution of the output spectra of the seven-wavelength mode-locking operation at a 2 h interval over 14 h, as shown in Fig. 7(c), indicating the long-term stability of the laser.

Furthermore, the seven-wavelength mode-locked pulses were also achieved when we increased the length of the SMF (L_{SMF}) from 20 to 135 m, and the pump strength was about 120 mW, as shown in Fig. 8. As seen from Fig. 8(b), the pulse train exhibited a period of about 680 ns, which implied that the fundamental repetition rate was ~ 1.47 MHz. Interestingly, we also observed the hybrid soliton pulses with the pump power of 270 mW. Figures 8(c) and 8(d) show the optical spectrum and the corresponding pulse train, respectively. Different from Fig. 6(b), the whole spectrum contained two parts. One part was a typical single-soliton spectrum with three pairs of Kelly sidebands, and its central wavelength and 3 dB spectral width were 1539.6 and ~1.2 nm, respectively. The other part was a four-wavelength mode-locking state around 1535 nm. Thus, we believe that it may be a five-wavelength mode-locked pulse. Figure 9 illustrates the linear-fitting relation between the average power and the

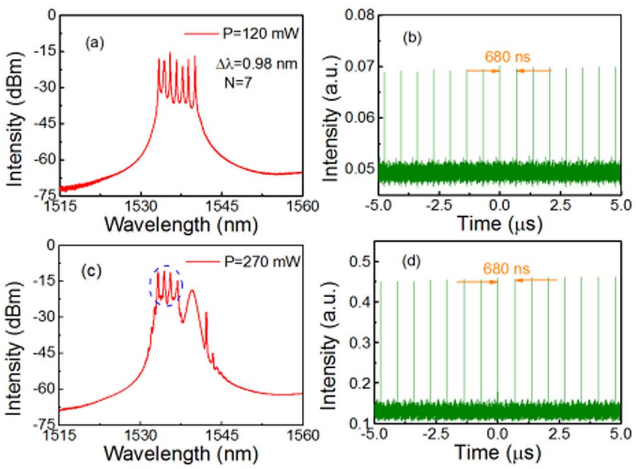

Fig. 8. Seven-wavelength and hybrid soliton operation with a length of SMF of 135 m and a corresponding cavity dispersion of $\sim -2.94\ ps^2$. (a), (c) The optical spectra and (b), (d) the corresponding pulse trains, respectively.

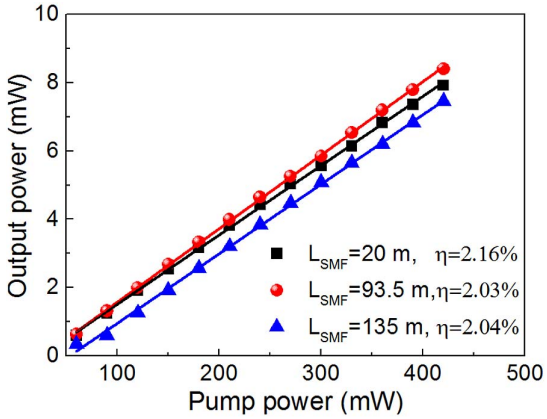

Fig. 9. Average output power versus the pump power of the laser with different lengths of SMF.

pump power. It can be seen that the maximum average output power and slope efficiency were 7.9 mW, 8.4 mW, 7.5 mW and 2.16%, 2.03%, 2.04% when L_{SMF} was 20 m, 93.5 m, and 135 m, respectively. According to the mode-locked theory, the corresponding pulse energies are 0.95 nJ, 4 nJ, and 5.1 nJ, respectively.

4.3. Discussion

The generation mechanism of multi-wavelength mode-locked pulses in the EDFL based on ULPGs can be explained as follows. As we know, multi-wavelength lasers are mostly based on the spectral-filtering principle, in which a comb filter is often used. In recent years, a large number of studies show that a cascaded long-period fiber grating has the function of comb filtering and has been used to realize multi-wavelength laser operation[44–46], which has been also verified by our work. In this experiment, the ULPG with seven tapers can be regarded as cascades of several short fiber gratings. Interestingly, the maximum number of wavelengths is seven, which may be related to the number of fiber tapers that compose the ULPG. We believe that because of the fiber tapers that compose the ULPG, by optimizing the parameters of the ULPG, including the grating length, grating period, diameter of the fiber core, and number of the fiber tapers, it is expected to obtain a laser with more wavelength numbers. It is worth noting that no matter how we adjust the gain, dispersion, and polarization state in the laser cavity, we have not found single- and dual-wavelength operation, which may be related to the highly nonlinear ULPG composed of seven fiber tapers[53–55]. In future work, we will further explore the formation mechanism of multiple wavelengths in ULPGs.

Meanwhile, we find that the ULPG also has the function of mode-locking and can be used as a mode-locker in fiber lasers, similar to long-period fiber gratings. For example, Intrachat and Kutz theoretically discovered passive mode-locking dynamics of a long-period fiber grating based on the mode-coupling theory and predicted that it could be used as a mode-locker[47]. Later, Karr *et al.* also discovered theoretically that many kinds of soliton pulses, including single soliton, bound soliton, long-period

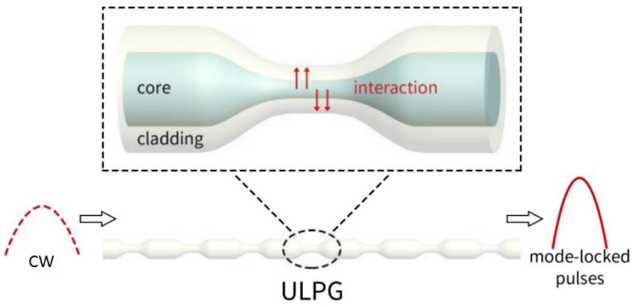

Fig. 10. Mode-locking principle of ULPG. CW, continuous wave.

pulsation, and multi-soliton pulse, may appear in a passively mode-locked EDFL with a long-period grating[48]. Therefore, the mode-locking principle of ULPG can be explained according to the above theory, as shown in Fig. 10. When the CW propagates in the ULPG, through the interaction between the core mode and the cladding mode, the low intensity part will be transferred to the cladding and attenuated, while its high-intensity part is not affected to a large extent due to resonance detuning under the high nonlinear effect. Thus, the mode-locked pulse is formed after many round trips in the laser cavity. In this experiment, the high nonlinearity provided by the seven-fiber taper plays an important role. It can be predicted that ULPG will become an ideal tool for studying the soliton phenomenon due to its dual functions of mode-locking and high nonlinearity in the future.

5. Conclusions

In conclusion, we have demonstrated a cascaded multi-wavelength mode-locked EDFL based on ULPG, in which the ULPG can be used as both a mode-locker and a comb filter to generate multi-wavelength mode-locked pulses. By taking advantage of the dual-function of the ULPG, three-, four-, five-, six-, and seven-wavelength mode-locked pulses are obtained in an all-fiber ring-cavity EDFL under the proper polarization states and pump strength. For the four-wavelength soliton pulse, its pulsewidth is about 7.8 ps. The maximum average output power, pulse energy, and slope efficiency of these pulses are 8.4 mW, 4 nJ, and 2.03%, respectively. Our study suggests that the ULPG could become a good candidate of pulse-shaping devices for a myriad of ultrafast photonic applications.

Acknowledgement

This work was supported by the Natural Science Foundation of Heilongjiang Province (No. JJ2019LH1509), National Natural Science Foundation of China (NSFC) (Nos. 11704086 and 61875043), Fundamental Research Funds for the Central Universities (No. 3072020CF2519), and 111 Project of Harbin Engineering University (No. B13015).

References

1. X. M. Liu, D. D. Han, Z. P. Sun, C. Zeng, H. Lu, D. Mao, and F. Q. Wang, "Versatile multi-wavelength ultrafast fiber laser mode-locked by carbon nanotubes," Sci. Rep. **3**, 2718 (2013).
2. Z. C. Luo, A. P. Luo, W. C. Xu, H. S. Yin, J. R. Liu, Q. Ye, and Z. J. Fang, "Tunable multiwavelength passively mode-locked fiber ring laser using intracavity birefringence-induced comb filter," IEEE Photon. J. **2**, 571 (2010).
3. Z. Y. Yan, X. H. Li, Y. L. Tang, P. P. Shum, X. Yu, Y. Zhang, and Q. J. Wang, "Tunable and switchable dual-wavelength Tm-doped mode-locked fiber laser by nonlinear polarization evolution," Opt. Express **23**, 4369 (2015).
4. Y. G. Han, T. V. A. Tran, and S. B. Lee, "Wavelength-spacing tunable multi-wavelength erbium-doped fiber laser based on four-wave mixing of dispersion-shifted fiber," Opt. Lett. **31**, 697 (2006).
5. Y. J. Yuan, Y. Yao, M. Yi, B. Guo, and J. J. Tian, "Multiwavelength fiber laser employing a nonlinear Brillouin optical loop mirror: experimental and numerical studies," Opt. Express **22**, 15352 (2014).
6. J. Yao, J. P. Yao, and Z. C. Deng, "Multiwavelength actively mode-locked fiber ring laser with suppressed homogeneous line broadening and reduced supermode noise," Opt. Express **12**, 4529 (2004).
7. Y. J. Song, L. Zhan, S. Hu, Q. H. Ye, and Y. X. Xia, "Tunable multiwavelength Brillouin-erbium fiber laser with a polarization-maintaining fiber Sagnac loop filter," IEEE Photon. Technol. Lett. **16**, 2015 (2004).
8. A. P. Luo, Z. C. Luo, and W. C. Xu, "Tunable and switchable multiwavelength erbium-doped fiber ring laser based on a modified dual-pass Mach–Zehnder interferometer," Opt. Lett. **34**, 2135 (2009).
9. J. B. Schlager, S. Kawanishi, and M. Saruwatari, "Dual-wavelength pulse generation using mode-locked erbium-doped fibre ring laser," Electron. Lett. **27**, 2072 (1991).
10. B. Bakhshi and P. A. Andrekson, "Dual-wavelength 10-GHz actively mode-locked erbium fiber laser," IEEE Photon. Technol. Lett. **11**, 1387 (1999).
11. V. J. Matsas, T. P. Newson, D. J. Richardson, and D. N. Payne, "Self-starting passively mode-locked fibre ring soliton laser exploiting nonlinear polarisation rotation," Electron. Lett. **28**, 1391 (1992).
12. D. U. Noske, M. J. Guy, K. Rottwitt, R. Kashyap, and J. R. Taylor, "Dual-wavelength operation of a passively mode-locked "figure-of-eight" ytterbium-erbium fibre soliton laser," Opt. Commun. **108**, 297 (1994).
13. H. Zhang, D. Y. Tang, X. Wu, and L. M. Zhao, "Multi-wavelength dissipative soliton operation of an erbium-doped fiber laser," Opt. Express **17**, 12692 (2009).
14. X. H. Li, K. Wu, Z. P. Sun, B. Meng, Y. G. Wang, Y. S. Wang, X. C. Yu, X. Yu, Y. Zhang, P. Shum, and Q. J. Wang, "Single-wall carbon nanotubes and graphene oxide-based saturable absorbers for low phase noise mode-locked fiber lasers," Sci. Rep. **6**, 25266 (2016).
15. Z. Q. Luo, J. Z. Wang, M. Zhou, H. Y. Xu, Z. P. Cai, and C. C. Ye, "Multiwavelength mode-locked erbium-doped fiber laser based on the interaction of graphene and fiber-taper evanescent field," Laser Phys. Lett. **9**, 229 (2012).
16. T. Zhu, Y. J. Rao, and J. L. Wang, "Characteristics of novel ultra-long-period fiber gratings fabricated by high-frequency CO_2 laser pulses," Opt. Commun. **277**, 84 (2007).
17. X. W. Shu, B. Gwandu, L. R. Zhang, and I. Bennion, "Ultra-long-period fiber gratings," Opt. Commun. **4**, 386 (2001).
18. X. W. Shu, L. Zhang, and I. Bennion, "Fabrication and characterisation of ultra-long-period fibre gratings," Opt. Commun. **203**, 277 (2002).
19. T. Zhu, Y. Song, Y. J. Rao, and Y. Zhu, "Highly sensitive optical refractometer based on edge-written ultra-long-period fiber grating formed by periodic grooves," IEEE Sensors J. **9**, 678 (2009).
20. E. Perez, H. M. Chan, I. V. Tomov, and H. P. Lee, "Fabrication of ultra-compact long-period fiber grating through a differentially scanned CO_2 laser," Proc. SPIE **31**, 6351 (2006).
21. Y. Liu and S. L. Qu, "Femtosecond laser pulses induced ultra-long-period fiber gratings for simultaneous measurement of high temperature and refractive index," Optik **124**, 1303 (2013).
22. S. P. Ugale and V. Mishra, "Formation and characterization of non-uniform long and ultralong period reversible optical fiber gratings," Optik **125**, 3822 (2014).
23. T. Almeida, R. Oliveira, P. André, A. Rocha, M. Facão, and R. Nogueira, "Automated technique to inscribe reproducible long-period gratings using a CO_2 laser splicer," Opt. Lett. **42**, 1994 (2017).

24. Y. Song, T. Zhu, Y. J. Rao, and Y. W. Zhao, "A humidity sensor based on ultra-long-period fiber gratings with asymmetric refractive index modulation," Chin. J. Lasers **36**, 2042 (2009).
25. B. Zou and K. S. Chang, "Phase retrieval from transmission spectrum for long-period fiber gratings," J. Lightwave Technol. **31**, 375 (2013).
26. L. Fang and H. Z. Jia, "Mode add/drop multiplexers of LP_{02} and LP_{03} modes with two parallel combinative long-period fiber gratings," Opt. Express **22**, 11488 (2014).
27. S. M. Israelsen and K. Rottwitt, "Broadband higher order mode conversion using chirped microbend long period gratings," Opt. Express **24**, 23969 (2016).
28. G. Masri, S. Shahal, A. Klein, H. Duadi, and M. Fridman, "Polarization dependence of asymmetric off-resonance long period fiber gratings," Opt. Express **24**, 29843 (2016).
29. H. Zhao, P. Wang, C. L. Zhu, R. Subramanian, and H. P. Li, "Analysis for the phase-diffusion effect in a phase-shifted helical long-period fiber grating and its pre-compensation," Opt. Express **25**, 19085 (2017).
30. W. Ni, P. Lu, C. Luo, X. Fu, D. Liu, and J. Zhang, "Simultaneous measurement of curvature and temperature based on thin core ultra-long-period fiber grating," in *2016 21st OptoElectronics and Communications Conference & 2016 International Conference on Photonics in Switching* (2016), p. 1.
31. T. Zhu, Y. J. Rao, and Q. J. Mo, "Simultaneous measurement of refractive index and temperature using a single ultra-long-period fiber grating," IEEE Photon. Technol. Lett. **17**, 744 (2005).
32. B. P. Shang, Y. P. Miao, H. M. Zhang, C. W. Fei, and L. J. Zu, "Ultralong-period microfiber grating for simultaneous measurement of displacement and temperature," IEEE Photon. Technol. Lett. **31**, 1763 (2019).
33. S. Zhang, S. F. Deng, T. Geng, C. T. Sun, and L. B. Yuan, "A miniature ultra-long period fiber grating for simultaneous measurement of axial strain and temperature," Opt. Laser Technol. **126**, 106121 (2020).
34. W. J. Ni, P. Lu, X. Fu, S. Wang, Y. Sun, D. M. Liu, and J. S. Zhang, "Highly sensitive optical fiber curvature and acoustic sensor based on thin core ultra-long period fiber grating," IEEE Photon. J. **9**, 7100909 (2017).
35. S. S. Zhang, C. Q. Fang, C. Zhang, J. Shi, and J. Q. Yao, "A compact ultra-long period fiber grating based on cascading up-tapers," IEEE Sens. J. **20**, 8552 (2020).
36. R. Slavík, Y. Park, M. Kulishov, and J. Azaña, "Terahertz-bandwidth high-order temporal differentiators based on phase-shifted long-period fiber gratings," Opt. Lett. **34**, 3116 (2009).
37. C. G. Tong, X. D. Chen, Y. Zhou, J. He, W. L. Yang, T. Geng, W. M. Sun, and L. B. Yuan, "Ultra-long-period fiber grating cascaded to a knob-taper for simultaneous measurement of strain and temperature," Opt. Rev. **25**, 295 (2018).
38. Y. H. Zhao, Y. Q. Liu, C. Y. Zhang, L. Zhang, G. J. Zheng, C. B. Mou, J. X. Wen, and T. Y. Wang, "All-fiber mode converter based on long-period fiber gratings written in few-mode fiber," Opt. Lett. **42**, 4708 (2017).
39. T. Erdogan, "Cladding-mode resonances in short-and long-period fiber grating filters," J. Opt. Soc. Am. A **14**, 1760 (1997).
40. R. Slavík, M. Kulishov, Y. Park, and J. Azaña, "Long-period-fiber-grating-based filter configuration enabling arbitrary linear filtering characteristics," Opt. Lett. **34**, 1045 (2009).
41. C. L. Zhu, H. Zhao, P. Wang, R. Subramanian, and H. P. Li, "Enhanced flat-top band-rejection filter based on reflective helical long-period fiber gratings," IEEE Photon. Technol. Lett. **29**, 964 (2017).
42. P. F. Wysocki, J. B. Judkins, R. P. Espindola, M. Andrejco, and A. M. Vengsarkar, "Broad-band erbium-doped fiber amplifier flattened beyond 40 nm using long-period grating filter," IEEE Photon. Technol. Lett. **9**, 1343 (1997).
43. Y. Zhou, K. Yan, R. S. Chen, C. Gu, L. X. Xu, A. T. Wang, and Q. Zhan, "Resonance efficiency enhancement for cylindrical vector fiber laser with optically induced long period grating," Appl. Phys. Lett. **110**, 161104 (2017).
44. Y. G. Han, C. S. Kim, J. U. Kang, U. C. Paek, and Y. Chung, "Multiwavelength Raman fiber-ring laser based on tunable cascaded long-period fiber gratings," IEEE Photon. Technol. Lett. **15**, 383 (2003).
45. M. Yan, S. Y. Luo, L. Zhan, Z. M. Zhang, and Y. X. Xia, "Triple-wavelength switchable erbium-doped fiber laser with cascaded asymmetric exposure long-period fiber gratings," Opt. Express **15**, 3685 (2007).
46. X. S. Liu, L. Zhan, S. Y. Luo, Y. X. Wang, and Q. S. Shen, "Individually switchable and widely tunable multiwavelength erbium-doped fiber laser based on cascaded mismatching long-period fiber gratings," J. Lightwave Technol. **29**, 3319 (2011).
47. K. Intrachat and J. N. Kutz, "Theory and simulation of passive mode-locking dynamics using a long-period fiber grating," IEEE J. Quantum. Electron. **39**, 1572 (2003).
48. A. S. Karar, T. Smy, and A. L. Steele, "Nonlinear dynamics of a passively mode-locked fiber laser containing a long-period fiber grating," IEEE J. Quantum. Electron. **44**, 254 (2008).
49. T. Geng, J. Li, W. L. Yang, M. W. An, H. Y. Zeng, F. Yang, Z. J. Cui, and L. B. Yuan, "Simultaneous measurement of temperature and strain using a long-period fiber grating with a micro-taper," Opt. Rev. **23**, 657 (2016).
50. B. Guo, Q. L. Xiao, S. H. Wang, and H. Zhang, "2D layered materials: synthesis, nonlinear optical properties and device applications," Laser Photon. Rev. **13**, 1800327 (2019).
51. B. K. Garside and T. K. Lim, "Laser mode locking using saturable absorbers," J. Appl. Phys. **44**, 2335 (1973).
52. W. S. Man, H. Y. Tam, M. S. Demokan, P. K. A. Wai, and D. Y. Tang, "Mechanism of intrinsic wavelength tuning and sideband asymmetry in a passively mode-locked soliton fiber ring laser," J. Opt. Soc. Am. B **17**, 28 (2000).
53. C. Baker and M. Rochette, "Highly nonlinear hybrid AsSe-PMMA microtapers," Opt. Express **18**, 12391 (2010).
54. H. N. Zhang, P. F. Ma, M. X. Zhu, W. F. Zhang, G. M. Wang, and S. G. Fu, "Palladium selenide as a broadband saturable absorber for ultra-fast photonics," Nanophotonics **9**, 2557 (2020).
55. G. P. Agrawal, *Nonlinear Fiber Optics*, 6th ed. (Academic Press, 2019).